



Cite this: *Chem. Commun.*, 2018, 54, 650

Received 2nd October 2017,  
Accepted 20th December 2017

DOI: 10.1039/c7cc07671a

rsc.li/chemcomm

## Microstructuration of poly(3-hexylthiophene) leads to bifunctional superhydrophobic and photoreactive surfaces†

L. Janovák,<sup>\*,a</sup> Á. Dernovics,<sup>a</sup> L. Mérai,<sup>a</sup> Á. Deák,<sup>a</sup> D. Sebők,<sup>a</sup> E. Csapó,<sup>ab</sup> A. Varga,<sup>ac</sup> I. Dékány<sup>ab</sup> and C. Janáky<sup>id</sup> <sup>\*,ac</sup>

**In this paper, we present the first report on an organic conducting polymer film, which alone exhibits both superhydrophobicity and visible light photoactivity. The microstructure of poly(3-hexylthiophene) was optimized using controlled precipitation until superhydrophobic behavior was achieved. Photocatalytic tests employing visible light irradiation proved that polymer degrades the ethanol test molecule.**

Controlling the wettability of solid surfaces and solid/fluid interfaces is important for a myriad of applications. Surfaces with water contact angles higher than 150° (superhydrophobicity) can exhibit self-cleaning effects, as found in lotus leaves in nature.<sup>1,2</sup> For preparing artificial superhydrophobic interfaces, hydrophobic functionality and surface roughness are both needed. Typically, a microstructure is superimposed by nanostructures, and this dual roughness reduces the contact area between water and the surface, resulting in water-repellent properties.<sup>3,4</sup> The second major class of self-cleaning surfaces is photocatalytic coatings, which chemically decompose organic pollutants upon light exposure – this process is known as photocatalysis.<sup>5</sup> The immobilization of photocatalyst nanoparticles in an appropriately structured binder or support material can lead to antimicrobial and self-cleaning properties, which expands the horizon of applications.

State-of-the-art bifunctional materials, possessing superhydrophobic and photoreactive properties,<sup>6</sup> are semiconductor photocatalyst/organic polymer nanocomposites.<sup>7,8</sup> In such assemblies, low-energy hydrophobic polymers are employed as inert matrices to immobilize photocatalysts, exploiting their flexibility, low weight,

impact resistance, and low cost.<sup>9–11</sup> At the same time, nano-composite configuration has considerable drawbacks. Most importantly, the polymer binder might decrease the intrinsic photocatalytic activity of the inorganic component *via* both optical/electrical shielding and by forming a physical barrier between the photoactive surface and the material to be decomposed. In addition, photogenerated charge carriers may also degrade the binder itself, causing possible detachment of the composite from the substrate.

In the search for conceptually new alternatives, conducting polymers (also called conjugated polymers or synthetic metals, CPs) deserve consideration as they may fulfil the above requirements alone, without the need for composite formation. The wettability of CPs depends greatly on their chemical structure and the used dopants.<sup>12</sup> For example, a polypyrrole (PPy) film containing a perfluorinated dopant anion exhibited hydrophobicity (water contact angle >90°), while ClO<sub>4</sub><sup>−</sup>-doped PPy was hydrophilic.<sup>13</sup> The synthesis of superhydrophobic CPs and the reversible control of their wettability between superhydrophobicity and superhydrophilicity were also demonstrated.<sup>14,15</sup> Although the photoactivity of CPs is well-known and has been exploited in organic solar photovoltaic<sup>16</sup> and photoelectrochemical cells,<sup>17</sup> photocatalytic studies of CPs alone (*i.e.*, without inorganic semiconductor particles) are still scarce.<sup>18</sup> In this vein, the photocatalytic activities of poly(diphenylbutadiyne) (PDPB), poly(3,4-ethylenedioxythiophene) (PEDOT), and P3HT were demonstrated under visible light irradiation without the assistance of sacrificial reagents or precious metal co-catalysts.<sup>19–21</sup>

In this communication, we demonstrate the facile preparation of a monolithic, microstructured organic conjugated polymer (P3HT) film, with adjustable surface roughness and visible light photoactivity. As the first step, P3HT was obtained *via* oxidative chemical polymerization.<sup>22</sup> The weight-average molecular weight of the as prepared P3HT was measured by a static light scattering method (104 500 g mol<sup>−1</sup>, Fig. S3a (ESI†) shows the respective Debye plot). In addition, viscosimetric measurements were carried out (employing the Mark–Kuhn–Houwink equation, Fig. S4, ESI†) which resulted in a very similar value ( $M_w = 101\,600$  g mol<sup>−1</sup>).

<sup>a</sup> Department of Physical Chemistry and Materials Science, University of Szeged, Rerrich B. tér 1, H-6720, Szeged, Hungary. E-mail: janovakl@chem.u-szeged.hu, janaky@chem.u-szeged.hu

<sup>b</sup> MTA-SZTE Biomimetic Systems Research Group, University of Szeged, Dóm tér 8, H-6720, Szeged, Hungary

<sup>c</sup> MTA-SZTE "Lendület" Photoelectrochemistry Research Group, University of Szeged, Rerrich Square 1, 6720 Szeged, Hungary

† Electronic supplementary information (ESI) available: Experimental details, analysis of the surface morphology and surface roughness, optical properties of the photoreactive films, and employed light sources are shown. See DOI: 10.1039/c7cc07671a



These values are in good agreement with other reports with a similar synthesis procedure ( $M_w = 80\,000\text{--}110\,000\text{ g mol}^{-1}$  measured by SEC and GPC).<sup>23,24</sup> The obtained P3HT was partially regioregular (rr) as deduced from the characteristic shoulders of the UV-vis spectrum (Fig. S5, ESI†). This notion was further confirmed by XRD measurements, where the P3HT films showed strong first-, second-, and third-order reflections at  $2\theta$  angles of 5.2, 10.6, and  $16.0^\circ$  (Fig. S6, ESI†). These reflections correspond to the crystalline, self-organized lamellar morphology, typically observed for rr-P3HT.<sup>25</sup>

Subsequently, P3HT films were prepared with a tailored morphology (and thus controlled hydrophilic properties) *via* controlled dissolution and reprecipitation. To obtain superhydrophobic surfaces ( $\theta > 150^\circ$ ) the flat surface must be roughened to further decrease the low surface free energy. The surface roughness of the P3HT layers can be adjusted under solvation conditions. In poor solvents, P3HT segments attract each other, and globular structures are formed to minimize the contact area between the polymer and the solvent. In good solvents, the size of the polymer coil is larger due to the better solvation of the macromolecule. After filtering such polymer solution/dispersions, the obtained films are very different: from a good solvent flat polymer films can be obtained, while the layer is rough in the case of a poor solvent (Fig. 1).

The chemically polymerized P3HT was soluble in toluene, but insoluble in DMF, and moderately soluble in a 60/40% v/v DMF/toluene mixture. The inserted photograph in Fig. 2 shows the P3HT polymer in this medium at different sonication times. At the beginning of the sonication process, P3HT formed a coarse dispersion with large polymer aggregates and the pale-yellow colour of the media is due to the low concentration of the dissolved polymer. During sonication, the larger polymer particles disaggregated, and the solubility of the polymer increased, while the particle size continuously decreased. The dark turbid samples at 5 and 10 min sonication indicate the small particles in the liquid with a high degree of dispersity. Consequently, the polymer particles gradually disappeared indicating an increased solvation of the polymer. After 30 min sonication, the heterogeneous system became a clear, homogenous,

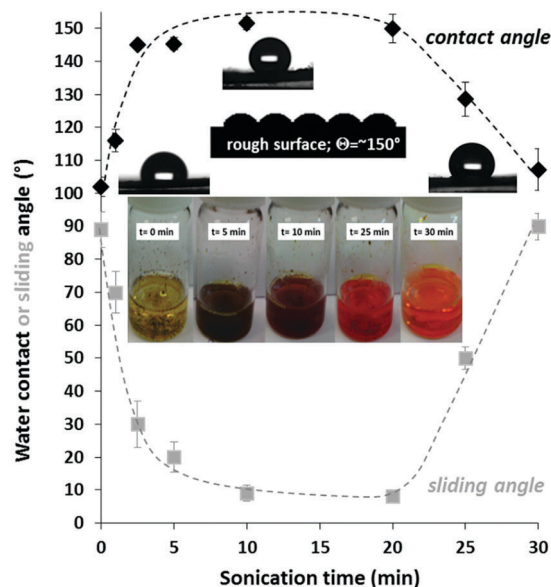


Fig. 2 The measured water contact and sliding angle values of P3HT films as a function of ultrasonication time in a 60/40% v/v DMF/toluene mixture ( $T = 25 \pm 0.5^\circ\text{C}$ ). The inserted picture shows the polymer dispersions after different sonication times. The dashed lines serve as a guide to the eye.

orange-coloured polymer solution without any insoluble particles. It is also noted that the applied sonication process degraded the polymer, because the molecular weight of the P3HT polymer decreased to  $74\,700\text{ g mol}^{-1}$  after 30 min sonication (Fig. S3b, ESI†).

SEM images were taken to monitor the surface morphology and roughness of the prepared functional films. Fig. 1 presents the SEM images of the P3HT films formed on a filter paper, by filtering the P3HT dispersion after different sonication times. After 1 min sonication (a) the surface of the P3HT was coarse, and the surface protrusions were mainly on the micrometer scale. After 5 min (b) and 10 min (c) sonication, however, the surface was well structured and roughened. This enhanced surface roughness completely disappeared after 30 min sonication, resulting in a smooth surface (d).

The above-presented microscale surface roughness was quantified by profilometry. Fig. S2 (ESI†) shows the microscale surface roughness ( $R_q$ ) values of the smooth and roughened P3HT layers. The measured  $R_q$  value of the flat P3HT layer was  $0.23 \pm 0.05\text{ }\mu\text{m}$ . The increasing sonication time resulted in a drastic increase in the surface roughness; for example, after 10 min sonication, an  $R_q$  value of  $7.85 \pm 0.60\text{ }\mu\text{m}$  was measured.

The polymer dispersion (or solution) was filtered through a filter paper after specific time intervals of sonication, and the wetting properties of the obtained films were determined. Fig. 2 shows the effect of sonication time on the measured contact angle values (black curve). The reason behind the witnessed maximum curve is that at a low sonication time the surface roughness was low because of the coarse micron-sized particles. After 10–20 min sonication, however, the particles were heterogeneous: besides micron-sized particles, polymer nanoparticles were also formed (Fig. S1, ESI†). In other words, the surface roughness of the low surface energy P3HT layer was increased

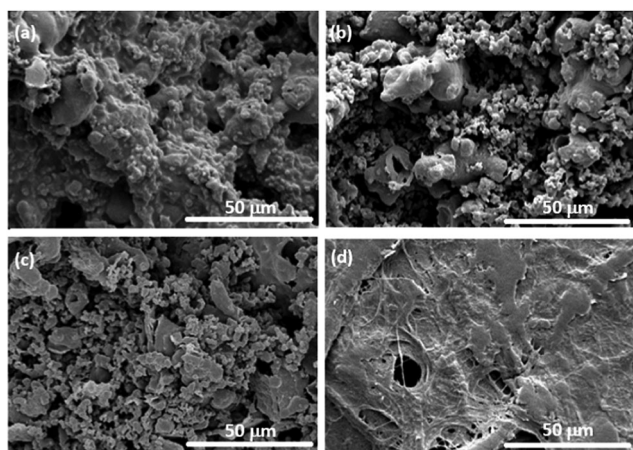


Fig. 1 SEM images of the P3HT films were formed on a filter paper after sonication for 1 min (a), 5 min (b), 10 min (c), and 30 min (d).



until a maximum contact angle was observed. Above this sonication time the polymer completely dissolved and consequently the surface roughness (and the contact angle) decreased. Besides the static water contact angle values, the sliding angles of the polymer surfaces were also measured (Fig. 2 with grey legends). The sliding angles of water droplets (25  $\mu$ l) decreased with increasing contact angles and the lowest sliding angle was less than  $10^\circ$  in the superhydrophobic region (as expected).<sup>26</sup> Notably, at the ideal sonication time (10–20 min), the obtained morphology (dual-roughness) is similar to the lotus leaf surface, which is known to reduce the contact area between water and the surface, resulting in water-repellent properties.<sup>27</sup>

Zisman analysis was performed with a set of different liquids with increasing surface tension to quantify the non-wettability of the low-energy P3HT surfaces. Zisman's method is based on the experimental finding that when a liquid spreads freely on a surface, its surface tension is lower or equal to that of the surface on which it is spreading.<sup>28</sup> For determining the surface free energy values, ethanol/water mixtures (0/100, 5/95, 15/85, 30/70, 40/60, and 100/0% v/v) with systematically increasing surface tension values (21.82, 32.98, 42.08, 55.73, and 72.01  $\text{mN m}^{-1}$ , respectively) were employed as test liquids. Fig. 3 presents the determined cosine value of contact angles as a function of liquid surface tensions. The dashed lines represent the best fits for the measured points and are extrapolated to intersect with the value of  $\cos \Theta_w = 1$  ( $\Theta = 0^\circ$ ).

At the point of intersection, a line can be drawn perpendicular to the x-axis, and the value of critical surface tension can be obtained. The determined surface free energy value of the flat P3HT polymer was  $19.8 \text{ mJ m}^{-2}$ , a value similar to that of the PTFE surface ( $20 \text{ mJ m}^{-2}$ ), measured as a reference.<sup>29</sup> Most importantly, the increase in the surface roughness of the P3HT caused a massive decrease in the measured surface energy value ( $16.4 \text{ mJ m}^{-2}$ ). The difference between the completely linear (PTFE) and hyperbolic

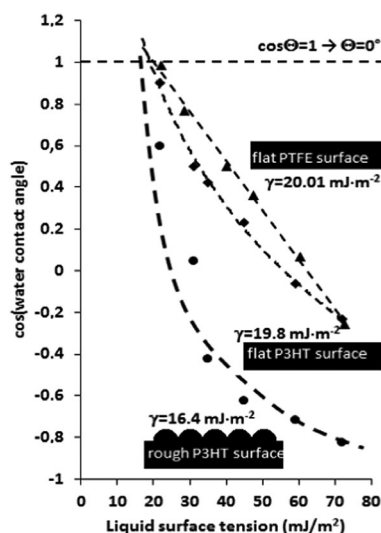


Fig. 3 Zisman plot for the flat P3HT layer and for the microstructured superhydrophobic layer with a rough surface ( $T = 25 \pm 0.5^\circ\text{C}$ ). The surface free energy of a conventional flat PTFE (Teflon) sample was also determined for reference.

(rough P3HT) shape of the measured curves is due to the different surface roughness and surface porosity. Notably, the hyperbolic nature of the Zisman plot is typical for rough superhydrophobic surfaces.<sup>30,31</sup> The superhydrophobic behaviour was also visualized by capturing a video about the water-repellent nature of the films (see the ESI†).

Before performing photocatalytic tests, the optical properties of the P3HT film were probed by UV-vis spectroscopy (Fig. S5, ESI†). The P3HT film had a broad absorption peak between 315 and 675 nm with a maximum of 515 nm, similarly to the precedent literature data.<sup>21,22</sup> Photodegradation of ethanol, used as a model volatile organic compound molecule was studied under both simulated sunlight and visible light, to probe the photocatalytic efficiency of the P3HT films (Fig. 4). Under simulated solar irradiation (a) the benchmark  $\text{TiO}_2$  film showed the highest photodegradation rate and after 180 min irradiation 57% of the initial 0.36 mM ethanol was photodegraded. In the case of roughened and smooth P3HT films these values were 38 and 31%, respectively. This trend is due to the UV component of the used solar simulator (Fig. S5, ESI†), which excites  $\text{TiO}_2$ . In contrast, under visible light irradiation ( $\lambda > 420 \text{ nm}$ ) the photocatalytic activity of the conventional P25  $\text{TiO}_2$  was negligible (Fig. 4b). On the other hand, P3HT films showed notable photocatalytic activity: after 180 min visible light irradiation, 44% of the initial ethanol amount was decomposed on the rough P3HT film.

Photooxidation of ethanol typically proceeds through the ethanol  $\rightarrow$  acetaldehyde  $\rightarrow$  acetic acid  $\rightarrow$  formaldehyde  $\rightarrow$  formic acid  $\rightarrow \text{CO}_2$  reaction pathway.<sup>32</sup> We also observed the formation of acetaldehyde, formaldehyde, acetic acid, formic acid and  $\text{CO}_2$  (as confirmed by GC analysis). The detailed analysis of these intermediates is not given in this communication, however, the concentrations of acetaldehyde as the main gas-phase intermediate and  $\text{CO}_2$  as the product are shown in Fig. S7 (ESI†). Acetaldehyde formation started at the beginning of irradiation, but mineralization of the main intermediate was not complete at the studied time interval. After about 90 min irradiation, the formation of  $\text{CO}_2$  was also detected. The photocatalytic degradation mechanism of phenol was studied on P3HT.<sup>21</sup> The formation of reactive oxygen species

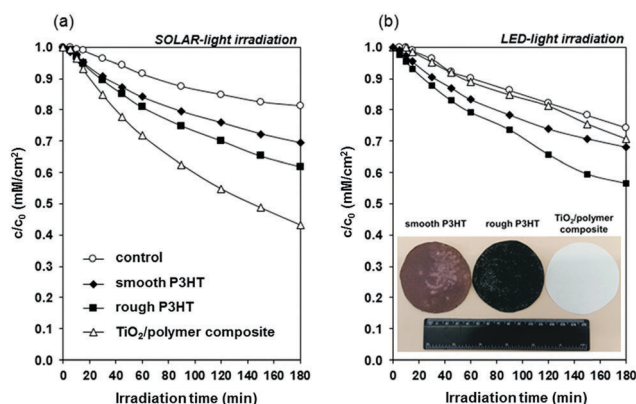


Fig. 4 Photocatalytic degradation rate of ethanol on smooth and rough P3HT films, compared with P25  $\text{TiO}_2$  as a function of illumination time under simulated solar (a) and LED-light (b) irradiation (solar  $\lambda = 280\text{--}900 \text{ nm}$  and LED  $\lambda = 420\text{--}700 \text{ nm}$ ). The inserted image represents the thin photoreactive films.



(ROS) ( $\text{HO}^\bullet$  and  $\text{O}_2^{\bullet-}$ ) was accounted to be responsible for the oxidation and degradation of the organic pollutants. In this reaction  $\text{O}_2^{\bullet-}$  was the main radical involved in the photocatalytic degradation. The measured difference between the photocatalytic efficiency of roughened and smooth polymer films is most likely rooted in the enhanced accessible photocatalytic surface area. The witnessed photocatalytic activity in the case of visible light irradiation is especially notable because only very low light intensity ( $\sim 1 \text{ mW cm}^{-2}$ ) was employed to mimic indoor conditions, where small light exposure is anticipated.

It is also an important question whether the formed ROS degrade the polymer itself? During this test, the P3HT film was illuminated with either simulated sunlight or visible LED light for one week under ambient conditions and the actual weight of the films was measured occasionally (Fig. S8, ESI†). The photocatalysis-induced weight loss of the polymer film was very pronounced in the case of solar light irradiation: after one week of continuous illumination, only a minor fraction of the initial polymer remained on the sample holder. In the case of visible LED light irradiation, however, the measured weight loss (*i.e.* the photocatalytic degradation of the polymer) was negligible.

In the search for self-cleaning surfaces there is a need to develop simple and efficient functional surfaces. To the best of our knowledge, in this communication we show the first experimental evidence of a monolithic conjugated polymer (P3HT) layer exhibiting visible light active photocatalytic and superhydrophobic properties, *i.e.* the one component monolithic polymer film shows dual water-repellent and photo-reactive properties. We demonstrated that the water repellent properties of P3HT films can be enhanced by increasing the surface roughness. Under optimal conditions, superhydrophobic behavior was achieved (see also the video in the ESI†). P3HT films were photoactive under visible light irradiation, which is particularly important for the future indoor applications, where the UV component of sunlight is filtered out by the windows. Elaborating on these proof-of-concept results, various members of the conjugated polymer family will be tested, and the examination of other practically relevant pollutants (including bacteria) will be performed.

The authors are very thankful for the financial support from the Hungarian Scientific Research Fund (OTKA) K 116323, NK 106234, PD 116224; and the project named GINOP-2.3.2-15-2016-00013. This paper was supported by the UNKP-17-4 New National Excellence Program of the Ministry of Human Capacities (L. J.).

## Conflicts of interest

There are no conflicts to declare.

## Notes and references

- 1 C. Kunlin, Z. Shuxue and W. Limin Wu, *Chem. Commun.*, 2014, **50**, 11891.
- 2 Y. Shen, G. Zhiguang and L. Weimin, *Chem. Commun.*, 2015, **51**, 1775.
- 3 P. A. Levkin, F. Svec and J. M. Fréchet, *Adv. Funct. Mater.*, 2009, **19**, 1993.
- 4 H. S. Lim, D. Kwak, D. Y. Lee, S. G. Lee and K. Cho, *J. Am. Chem. Soc.*, 2007, **129**, 4128.
- 5 K. Rajeshwar, A. Thomas and C. Janáky, *J. Phys. Chem. Lett.*, 2015, **6**, 139.
- 6 Á. Deák, L. Janovák, E. Csapó, D. Ungor, I. Pálkó, S. Puskás, T. Ördög, T. Ricza and I. Dékány, *Appl. Surf. Sci.*, 2016, **389**, 294.
- 7 T. Kamegawa, Y. Shimizu and H. Yamashita, *Adv. Mater.*, 2012, **27**, 3697.
- 8 S. Nishimoto and B. Bhushan, *RSC Adv.*, 2013, **3**, 671.
- 9 W. Zhang, X. Lu, Z. Xin and C. Zhou, *Nanoscale*, 2015, **7**, 19476.
- 10 J. H. Lee, E. J. Park, D. H. Kim, M. G. Jeong and Y. D. Kim, *Catal. Today*, 2016, **260**, 32–38.
- 11 P. A. Charpentier, K. Burgess, L. Wang, R. R. Chowdhury, A. F. Lotus and G. Moula, *Nanotechnology*, 2012, **23**, 425606.
- 12 A. Azioune, M. M. Chehimi, B. Miksa, T. Basinska and S. Slomkowski, *Langmuir*, 2002, **18**, 1150.
- 13 D. Mecerreyes, V. Alvaro, I. Cantero, M. Bengoetxea, P. A. Calvo, H. Grande, J. Rodriguez and J. A. Pomposo, *Adv. Mater.*, 2002, **14**, 749.
- 14 L. Xu, W. Chen, A. Mulchandani and Y. Yan, *Angew. Chem., Int. Ed.*, 2005, **44**, 6009.
- 15 N. R. Chiou, C. Lu, J. Guan, L. J. Lee and A. J. Epstein, *Nat. Nanotechnol.*, 2007, **2**, 354.
- 16 S. Günes, H. Neugebauer and N. S. Sariciftci, *Chem. Rev.*, 2007, **107**, 1324.
- 17 D. Hursán, A. Kormányos, K. Rajeshwar and C. Janáky, *Chem. Commun.*, 2016, **52**, 8858.
- 18 B. Muktha, G. Madras, T. N. Guru Row, U. Scherf and S. Patil, *J. Phys. Chem. B*, 2007, **111**, 7994.
- 19 S. Ghosh, N. A. Kouamé, L. Ramos, S. Remita, A. Dazzi, A. Deniset-Besseau, P. Beaunier, F. Goubard, P. H. Aubert and H. Remita, *Nat. Mater.*, 2015, **14**, 505.
- 20 S. Ghosh, N. A. Kouame, S. Remita, L. Ramos, F. Goubard, P. H. Aubert, A. Dazzi, A. Deniset-Besseau and H. Remita, *Sci. Rep.*, 2015, **5**, 18002.
- 21 D. Floresyona, F. Goubard, P. H. Aubert, I. Lampre, J. Mathurin, A. Dazzi, S. Ghosh, P. Beaunier, F. Brisset, S. Remita, L. Ramos and H. Remita, *Appl. Catal., B*, 2017, **209**, 23.
- 22 A. Varga, B. Endródi, V. Hornok, C. Visy and C. Janáky, *J. Phys. Chem. C*, 2015, **119**, 28020.
- 23 S. Amou, O. Haba, K. Shirato, T. Hayakawa, M. Ueda, K. Takeuchi and M. Asai, *J. Polym. Sci., Part A: Polym. Chem.*, 1999, **37**, 1943.
- 24 T. A. P. Hai and R. Sugimoto, *J. Mol. Struct.*, 2017, **1146**, 660.
- 25 T.-A. Chen, X. Wu and R. D. Rieke, *J. Am. Chem. Soc.*, 1995, **117**, 233.
- 26 M. Miwa, A. Nakajima, A. Fujishima, K. Hashimoto and T. Watanabe, *Langmuir*, 2000, **16**, 5754.
- 27 R. Nishimura, K. Hyodo, H. Sawaguchi, Y. Yamamoto, Y. Nonomura, H. Mayama, S. Yokojima, S. Nakamura and K. Uchida, *J. Am. Chem. Soc.*, 2016, **138**, 10299.
- 28 W. A. Zisman, *Adv. Chem. Ser.*, 1964, **43**, 1.
- 29 H. Tavana, F. Simon, K. Grundke, D. Y. Kwok, M. L. Hair and A. W. Neumann, *J. Colloid Interface Sci.*, 2005, **291**, 497.
- 30 T. Bharathidasan, T. N. Narayanan, S. Sathyanarayanan and S. S. Sreejakumari, *Carbon*, 2015, **84**, 207.
- 31 S. Sutha, S. C. Vanithakumari, R. P. George, U. K. Mudali, B. Raj and K. R. Ravi, *Appl. Surf. Sci.*, 2015, **347**, 839.
- 32 M. R. Nimlos, E. J. Wolfrum, M. L. Brewer, J. A. Fennell and G. Bintner, *Environ. Sci. Technol.*, 1996, **30**, 3102.

